ON-LINE APPENDIX

Assessment of the Similarity of DEC Maps and Tractography Reconstructions among Different DWI Schemes Used in This Study

This study consists of analyzing DWI data acquired from 3 different sites, using different acquisition protocols and MR imaging scanners. The patient DWI data were from 2 participating institutions (E. Medea Institute, Italy, and Royal Children's Hospital, Australia), and the control MR imaging data were from a public repository (PedsDTI, National Institutes of Health; https://pediatricmri.nih.gov/nihpd/info/index.html). The scanner details, and sequence parameters used for the 3 acquisition protocols are summarized in On-line Table 1.

To investigate the interscanner and intersite variance of tractography reconstructions and to minimize the confounding introduced in assessing the WMT morphology, we examined the variations in tractography appearance by acquiring data from a single healthy control, using all 3 DWI acquisition schemes (using the same 3T MR imaging scanner used for patients from each participating institution and a 1.5T MR imaging scanner from the Milan Children's Hospital). The 3 datasets were processed according to the methods described in the main text. The derived DEC maps and the selected WMT tractography were then carefully assessed and compared visually by one of the study neuroradiologists (F.A.).

The DEC map appearance and the gross morphology of reconstructed WMTs were comparable among the 3 datasets. There were minor differences emerging in the peripheral branches of the WMTs, which were not evaluated by the scoring system used for the MCD cases.

This analysis confirmed that the interscanner and intersite variance of different DWI acquisitions did not substantially affect the appearance of the derived DEC maps and WMT tractography reconstructions. On-line Figs 1 and 2 demonstrate the DEC maps and selected WMT tractography images from the 3 datasets.

On-line Table 1: Summaries of the MR imaging protocols used

	E. Medea Institute	Royal Children's Hospital	PedsDTI Data Base
No. of cases	43	7	101
Scanner manufacturer	Achieva, Philips Healthcare	Magnetom Trio, Siemens	Magnetom Trio, Siemens; SIGNA, GE Healthcare
Field strength	3T	3T	1.5T
T1WI[a]	MPRAGE; FOV = 240 × 200 mm; 1.0-mm^3 isotropic voxels	MPRAGE; FOV = 250 × 250 mm; 0.8-mm^3 isotropic voxels	3D echo-spoiled gradient echo (or spin-echo for subjects younger than 4.5 years of age); FOV = 256 × 180; 1.0-mm^3 isotropic voxels (or 1.0 × 1.0 × 3.0 mm for subjects younger than 4.5 years of age)
T2WI[a]	TSE; FOV = 230 × 230 mm; resolution = 0.23 × 0.23 × 3 mm	TSE; FOV = 165 × 220 mm; resolution = 0.4 × 0.4 × 2.5 mm	TSE; FOV = 256 × 224 mm; resolution = 1 × 1 × 2/3 mm
DWI	EPI, 32 noncollinear DW directions; b-values = 0, 1100 s/mm^2; No. of B_0 volumes = 8; 29 cases had phase-reversed blip DWI; 2.2-mm^3 isotropic voxels; acquisition: TR/TE = 8800/100 ms; FOV = 246 × 246 mm; 80 slices	Two different acquisition protocols were used. Acquisition 1 (SB-HARDI) on 5 patients: PGSE-SSEPI, 60 noncollinear DW directions; b-values = 0, 3000 s/mm^2; No. of B_0 volumes = 7; 2.3-mm^3 isotropic voxels; TR/TE = 7600/110 ms; FOV = 240 × 24 mm; 54 slices Acquisition 2 (MB-HARDI) on 2 patients: PGSE-SSEPI, 60 noncollinear DW directions; b-values = 0, 2800 seconds/mm^2; No. of B_0 volumes = 10; a pair of reversed-phase polarity B_0; 2.4-mm^3 isotropic voxels; MB factor = 3; TR/TE = 3200/110 ms; FOV = 260 × 260 mm; 2.4-mm isotropic voxels; 63 slices	EPI, 50 noncollinear DW directions; b-values = 0, 1100 s/mm^2; No. of B_0 volumes = 10; 2.5-mm^3 isotropic resolution; TR/TE = 3000/87 ms; FOV = 240× 240 mm; 96 × 96 matrix; 60 slices

Note:—SB-HARDI indicates single-band HARDI; MB-HARDI, multiband HARDI; PGSE, pulse gradient spin-echo; SSEPI, single-shot echo-planar imaging; DW, diffusion weighted; MF, multi-band.

[a] TR and TE on each scanner were set according to subjects' ages.

On-line Table 2: The demographics and age-grouping details of the typically developing children's MR imaging data used to generate the study's healthy control templates

Template	No. of Subjects	M/F	Mean Age (yr)	Age SD (yr)	Age Range (yr)	Age (yr) (No.) of Patients Compared with the Template
1	12	6:6	1.5	0.7	0.8–3	1.4 (1)
2	10	4:6	2.0	0.8	1–3.1	1.9–2.8 (7)
3	10	7:3	4.5	1.1	3–5.8	3.2–5.4 (11)
4	11	6:5	6.7	1.1	5.2–8.1	5.8–8.4 (13)
5	24	12:12	11.9	0.5	11.1–12.9	9.4–13 (9)
6	22	10:12	15.0	0.7	13.6–16	13.4–16 (5)
7	27	14:13	19.8	1.0	18.2–21.5	17.9–21.2 (4)

On-line Table 3: Confirmed genetic diagnosis in the 11 study cases

Gene Mutations	No. of Cases
DYNC1H1	2
OFD1	1
GPR56	1
KIF5C	1
RAB3GAP1	1
TBR1	1
TUBB2B	1
TUBA1A	1
WDR62	1
Deletion on Xp23 involving *DCX*, *PAK3*, and *CAPN6*	1

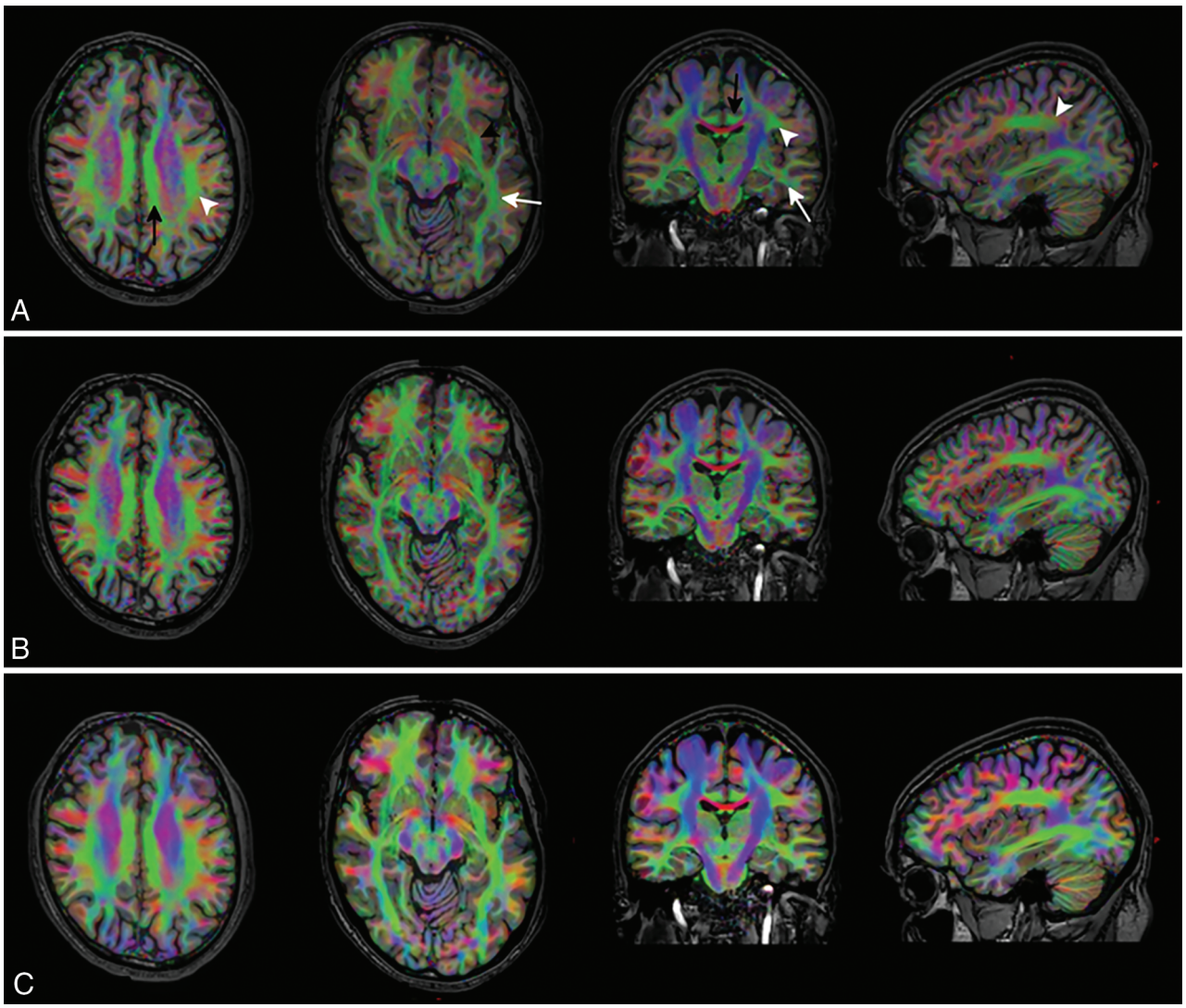

ON-LINE FIG 1. Comparison of the direction-encoded color maps computed from diffusion-weighted imaging data acquired with the PedsDTI (*A*), E. Medea Institute (*B*), and Royal Children's Hospital (*C*) protocols on the same healthy subject. The superior longitudinal fasciculus (*white arrowheads*), inferior fronto-occipital fasciculus (*black arrowhead*), inferior longitudinal fasciculus (*white arrows*), and cingulum (*black arrows*) can be identified on all the datasets, showing a similar color appearance, representing the estimated local fiber orientation distribution.

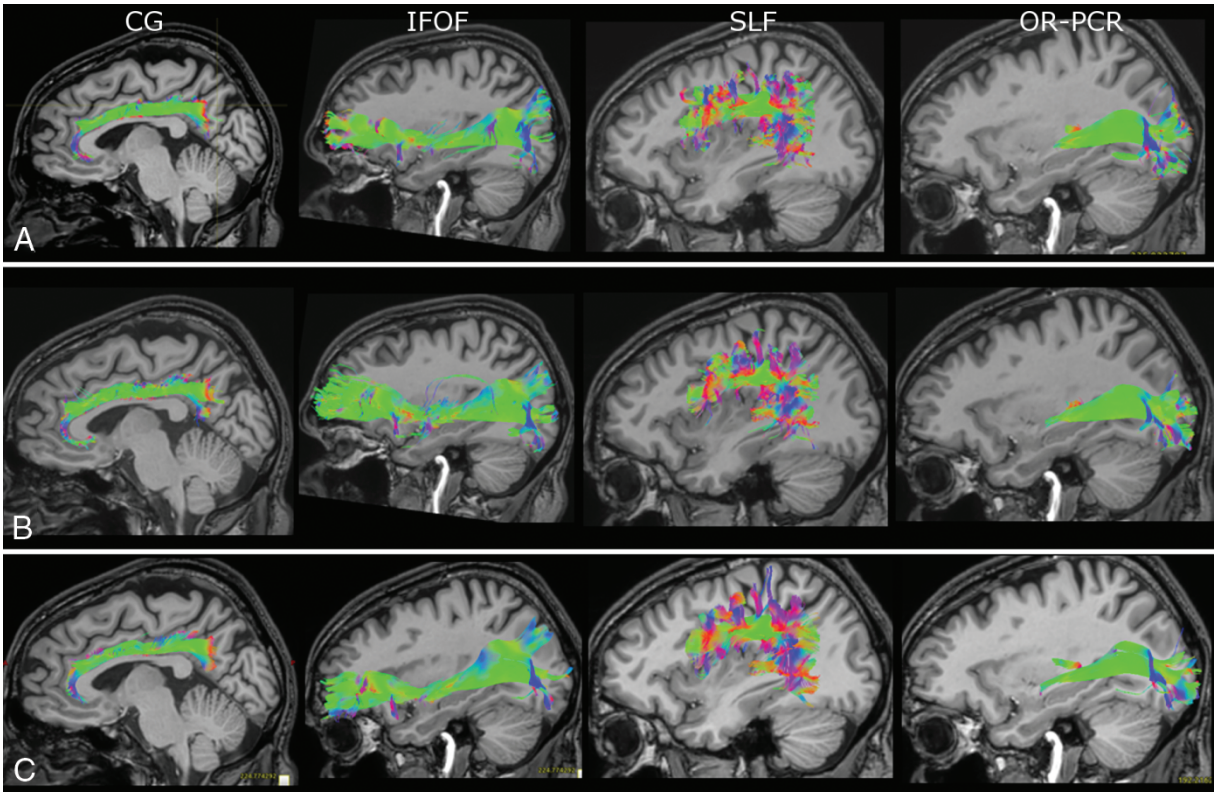

ON-LINE FIG 2. Comparison of the selected tractography images reconstructed using diffusion-weighted imaging data acquired with the PedsDTI (*A*), E. Medea Institute (*B*), and Royal Children's Hospital (*C*) protocols on the same healthy subject. The tractography examples, (from left to right) cingulum, inferior fronto-occipital fasciculus, superior longitudinal fasciculus, and optic radiation-posterior corona radiata, demonstrate a similar gross tract profile and tract morphology, among the different datasets.

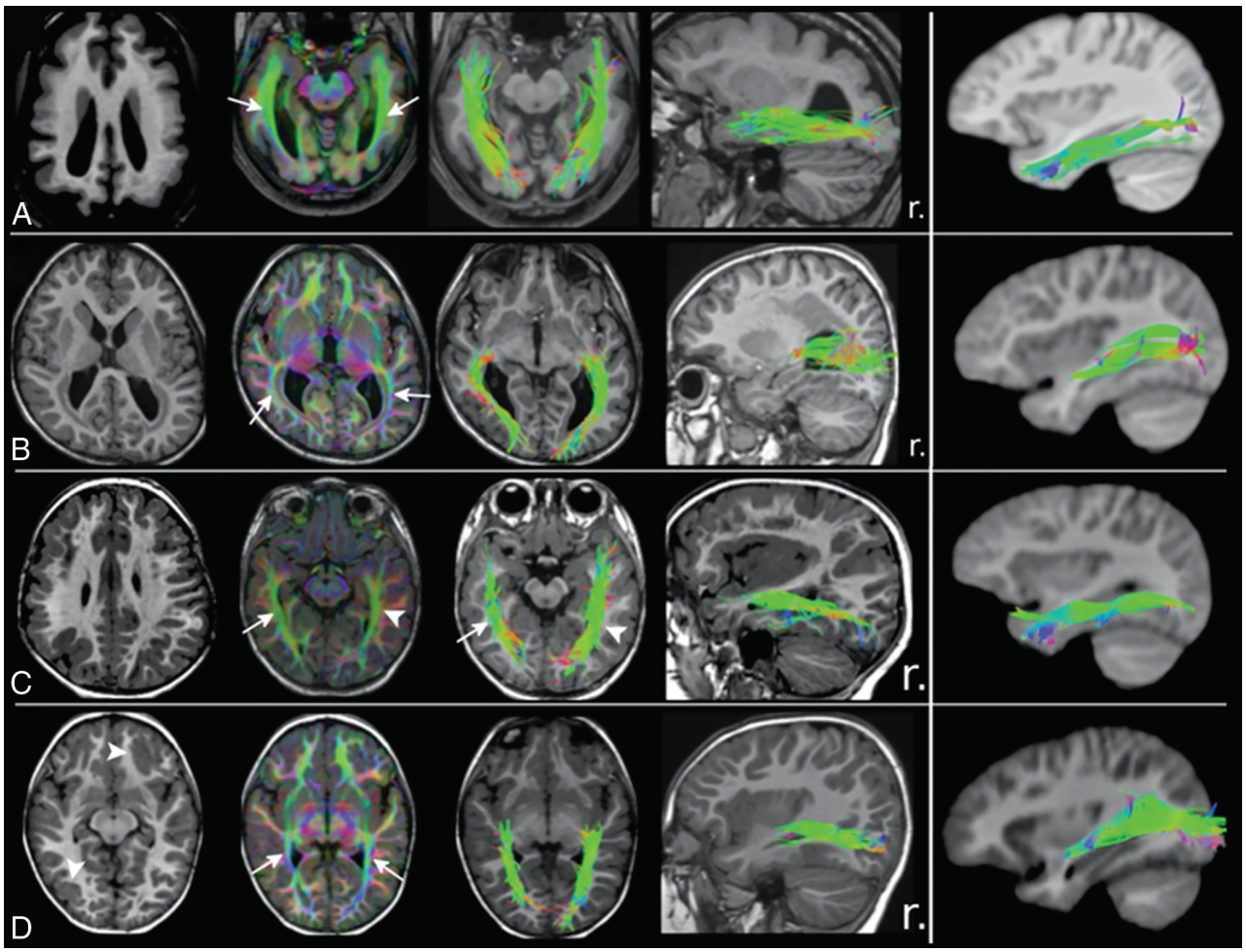

ON-LINE FIG 3. Additional tractography findings in patients with lissencephaly and polymicrogyria. T1WI, direction-encoded color maps, and tractography reconstructions in 2 patients with LIS (*A* and *B*) and 2 with PMG (*C* and *D*) are shown. For each patient, a comparable tractography reconstruction from the age-matched healthy control template is shown in the last column for comparison. *A*, An irregular (distorted) bilateral inferior longitudinal fasciculus in a subject with pachygyria and thin subcortical band heterotopia. *B*, Irregular (smaller and distorted) optic radiation–posterior corona radiata (*arrows* on DEC map) in a patient with SBH with no pachygyria. *C*, Irregular (thinner and shorter) right ILF (*arrows*) in a patient with unilateral right frontoparietal PMG. The left ILF (*arrowheads*) has a normal appearance. *D*, Irregular (thinner and shorter) OR-PCR (*arrows* on the DEC map) in a patient with multifocal (right occipital, left frontal) PMG (*arrowheads*). r. indicates right.

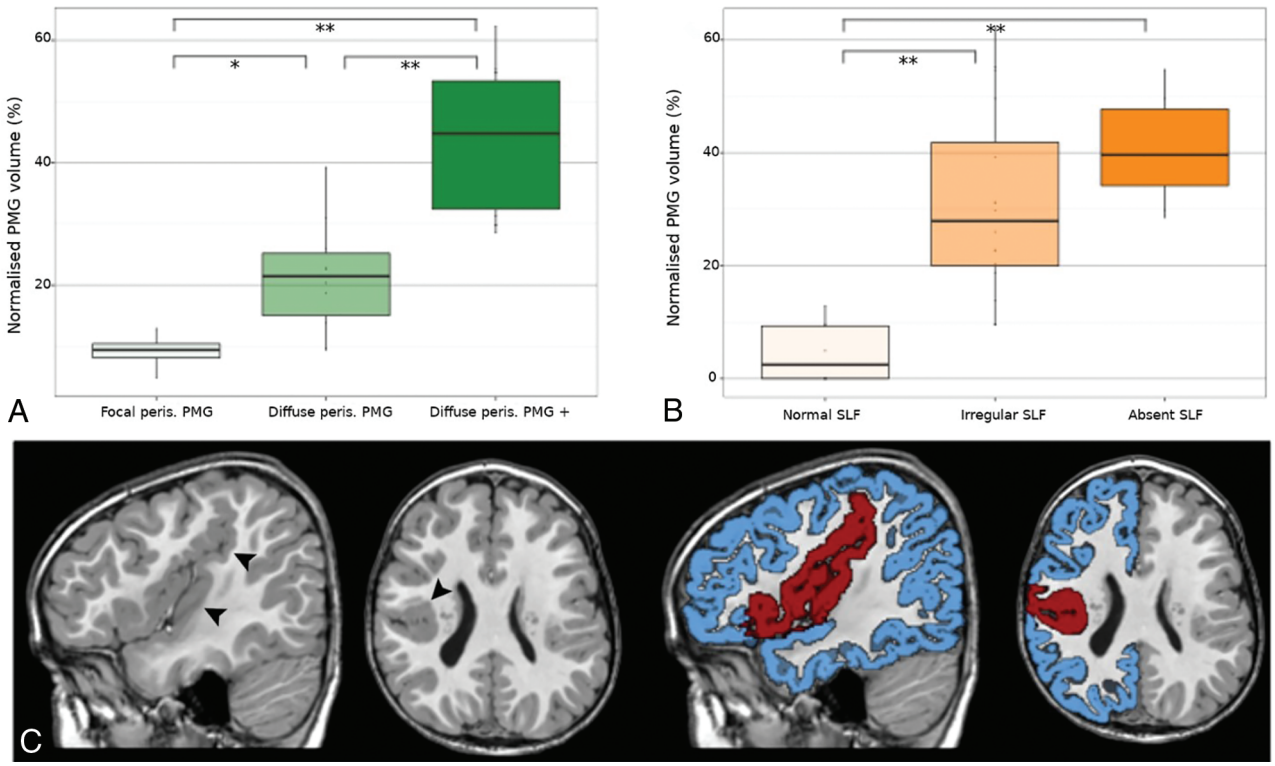

ON-LINE FIG 4. Volumetric analysis in peri-Sylvian polymicrogyria and association with the superior longitudinal fasciculus structural abnormalities. *Boxplot A* shows the normalized PMG cortical volumes (expressed as a percentage of the total cortical ribbon volume from the ipsilateral hemisphere) by peri-Sylvian PMG subgroups (focal, diffuse, and diffuse plus adjacent cortical PMG) in the 16 patients with peri-Sylvian PMG. *Boxplot B* shows the normalized PMG cortical volumes by the SLF tractography appearance (normal, irregular, and absent SLFs). Significant differences of PMG volumes on pair-wise *t* tests between the PMG subgroups (in *A*) and the different SLF appearance (in *B*) are reported: *Asterisk* indicates $P < .05$; *2 asterisks*, $P < .01$. *C*, The T1-weighted images of a patient with diffuse peri-Sylvian PMG (*black arrowhead*) showing the FreeSurfer-based (http://surfer.nmr.mgh.harvard.edu) cortical ribbon segmentation (in *blue*) and expert manual tracing of the malformed cortex (in *red*) by the study neuroradiologist (F.A.). Peris. indicates peri-Sylvian.

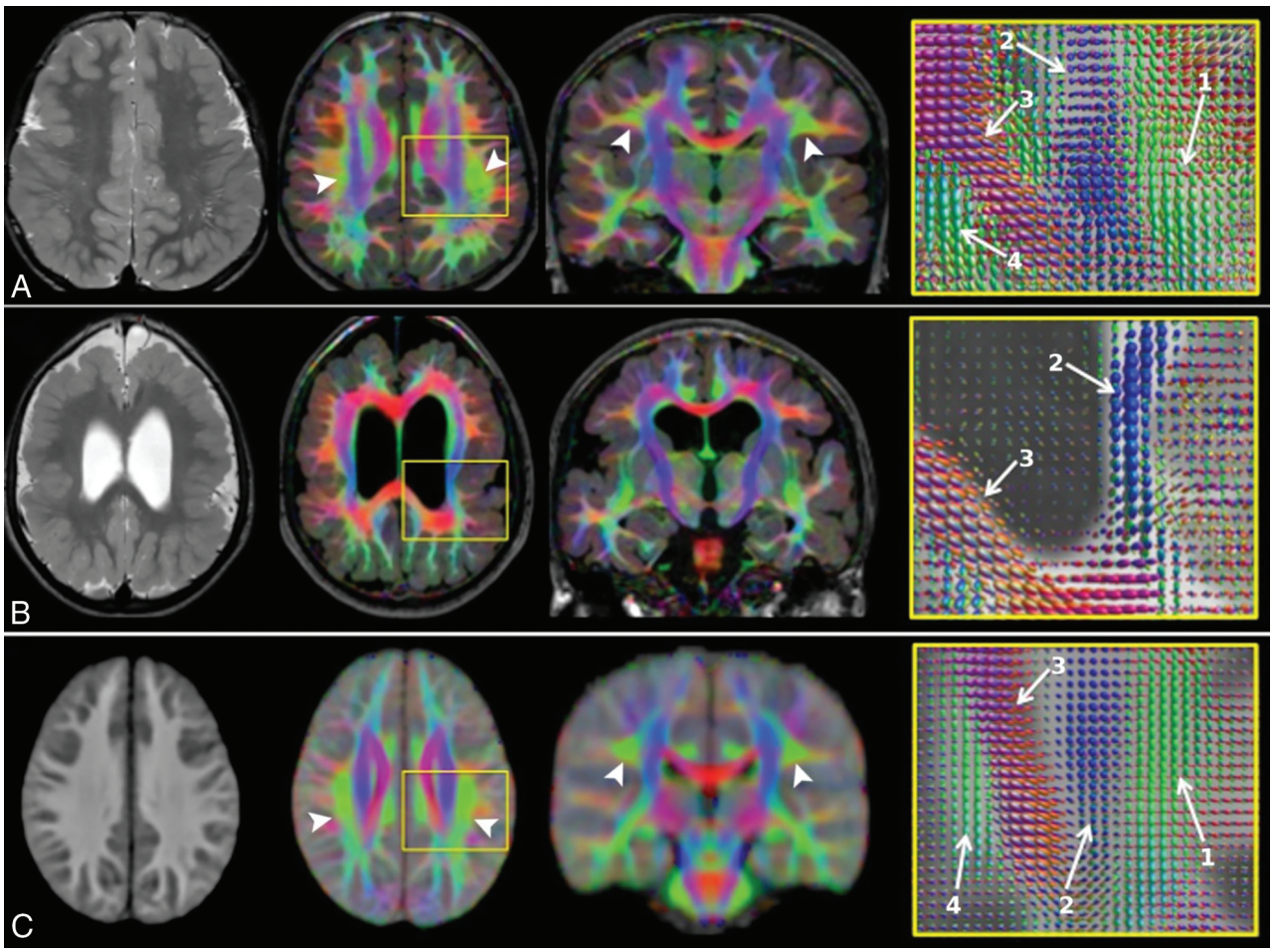

ON-LINE FIG 5. The superior longitudinal fasciculus appearance in patients with congenital cytomegalovirus infection. T1WI, direction-encoded color maps, and fiber orientation distribution glyph profiles in the deep white matter regions containing the SLF are shown in the following: *A*, A patient with generalized polymicrogyria related to a prenatal CMV infection. *B*, A patient with generalized PMG not related to a CMV infection. *C*, The age-matched healthy control template for comparison. Patient A demonstrates a normal-appearing left SLF and an irregular (thinned) right SLF (*arrowheads*). Patient B has bilateral SLF agenesis. On the FOD glyph maps, 1 indicates SLF (green, predominately anterior-posterior-oriented fiber distribution); 2, corona radiata (blue, predominantly superior-inferior-oriented fiber distribution); 3, corpus callosum (red, predominately left-right-oriented fiber distribution); and 4, cingulum (green, predominately anterior-posterior-oriented fiber distribution).